PCCP

PAPER

View Article Online
View Journal | View Issue

Cite this: *Phys. Chem. Chem. Phys.*, 2025, **27**, 7375

Molecular heaters: a green route to boosting crop yields?†‡

Jack M. Woolley, ‡[a] Natercia D. N. Rodrigues, ‡[a] Josene M. Toldo, ‡*[b] Benjamin Rioux, ‡[c] Chris Groves,‡[d] Xandra Schrama,‡[e] Jimmy Alarcan,‡[f] Temitope T. Abiola,[a] Matthieu M. Mention,[c] Mariana T. do Casal,[b] Simon E. Greenough,[a] Marise Borja,[g] Wybren J. Buma, *[hi] Michael N. R. Ashfold, *[j] Albert Braeuning,*[f] Teun Munnik,*[e] Keara A. Franklin,*[d] Florent Allais, *[c] Mario Barbatti [bk] and Vasilios G. Stavros*[al]

Received 20th December 2024,
Accepted 17th March 2025

DOI: 10.1039/d4cp04803b

rsc.li/pccp

Food production and food security are fast becoming some of the most pressing issues of the 21st century. We are developing environmentally responsible molecular heaters to help boost crop growth and expand geographic areas capable of supporting growth. Sinapic diacid (SDA) is such a molecule, that can act as a light-to-heat agent, converting solar energy into heat delivered to the plant. We have characterised the photophysical properties of SDA extensively, using a combination of steady-state and ultrafast laser spectroscopy techniques complemented with high-level computational studies, and demonstrated both its resilience to prolonged solar irradiation and light-to-heat capabilities. The results we present here illustrate the untapped potential of molecular heaters such as SDA to boost plant yields in existing growing regions and to expand growth into regions hitherto considered too cold for crop growth.

Introduction

Global warming is leading to increased temperatures and extreme weather events in most regions of the world,[1] placing well recognised stresses on local crop production.[2] Temperature stress and general climate instability all have adverse effects on plant growth and crop yields.[3,4] Mitigating the adverse effects of changing climate is an essential step towards improved food security, in line with Goal 2 of the United Nations' Sustainable Development Goals for 2030 and the Zero Hunger initiative by the United Nations' Department of Economic and Social Affairs.[5] From a geographic perspective, one obvious change is that regions with a climate suitable for growth of a particular crop are shifting further from the equator – as exemplified by the rapid increase in grape and wine production in the south east of the UK.[6,7]

Temperature, just one of many factors affecting successful plant growth, is the focus of the present study wherein we report the development of a new category of molecular heater that could be applied to the leaves of plants by a water-based foliar spray. The potential benefits of such technology are manifold. In geographic regions that are currently suitable for growth, a modest increase in temperature could boost plant growth and yields, as well as protect them against sharp and sudden decreases in temperature, known as cold snaps. In addition, the same modest increase in temperature could also allow a given crop to flourish in slightly cooler geographic regions (further north/south, or at higher elevation), ultimately extending arable areas.

Molecular heaters convert photon energy afforded by absorption of ultraviolet radiation (UVR, 280–400 nm) to thermal energy (heat) through an efficient, energy-conserving relaxation mechanism. They have many photophysical characteristics in common with organic sunscreen molecules, whose primary role is to block incident UV radiation.[8] The resulting

[a] *Department of Chemistry, University of Warwick, Coventry, CV4 7AL, UK. E-mail: v.stavros@bham.ac.uk*
[b] *Aix Marseille University, CNRS, ICR, Marseille, France*
[c] *URD, Agro-Biotechnologies Industrielles (ABI), CEBB AgroParisTech, 51110 Pomacle, France*
[d] *School of Biological Sciences, University of Bristol, Bristol, BS8 1TQ, UK*
[e] *Section Plant Cell Biology, University of Amsterdam, Amsterdam, The Netherlands*
[f] *Department of Food Safety, German Federal Institute for Risk Assessment, Max-Dohrn-Str. 8-10, 10589, Berlin, Germany*
[g] *GAB Consulting Spain S.L.U., Calle Gregorio Mayans 3, pta. 10 46005 Valencia, Spain*
[h] *Van 't Hoff Institute for Molecular Sciences, University of Amsterdam, Amsterdam, The Netherlands*
[i] *Institute for Molecules and Materials, FELIX Laboratory, Radboud University, 6525 ED Nijmegen, The Netherlands*
[j] *School of Chemistry, University of Bristol, Cantocks Close, Bristol, BS8 1TS, UK*
[k] *Institut Universitaire de France, 75231 Paris, France*
[l] *School of Chemistry, University of Birmingham, Birmingham, B15 2TT, UK*

† Electronic supplementary information (ESI) available. See DOI: https://doi.org/10.1039/d4cp04803b

‡ These authors contributed equally.

heat in the case of organic sunscreen molecules is an unwanted by-product, whereas it is the primary motivation in the case of a molecular heater for enhancing plant growth. The exemplar molecule reported here is sinapic diacid (SDA, 2-(4-hydroxy-3,5-dimethoxybenzylidene)malonic acid). Other materials that have been shown to offer light-to-heat conversion capability include extensive structures like graphene, carbon nanotubes and Ti_3C_2, generally targeting solar driven water evaporation.[9–12]

A molecular heater for application in agriculture must meet several key criteria. First, it should absorb solar radiation efficiently in a region of the electromagnetic spectrum that does not overlap with that required for photosynthesis.[13] Second, it should be able to dissipate the energy gained by absorbing solar radiation into heat with close-to-unity quantum yields across the range of environments to which it is exposed. Finally, and crucially, it needs to be developed into a cost-effective formulation, the application of which needs to be relatively facile, and the product must have no adverse effect on the plant physiology or the surrounding environment, which requires that it must be non-toxic to the soil, water, humans, and other animals.

Here we report on the results of studies employing a broad suite of techniques, designed to test the effectiveness of SDA as a proposed molecular heater intended for use in agriculture. SDA, the structure of which is shown in the inset of Fig. 1, is produced through a green chemistry method.[14] Ultrafast transient absorption spectroscopy (TAS) has been used in tandem with time-dependent density functional theory (TD-DFT) to elucidate the photodynamics of SDA across a range of environments in which the molecular heater is intended to operate. Comparative photostability studies are reported for a collection of structurally similar molecules, that illustrate and identify the fitness of SDA. The present studies of SDA are performed as a proof of concept, that highlights the potential for expanding molecular heater technology, using structurally similar systems to address a major societal challenge.

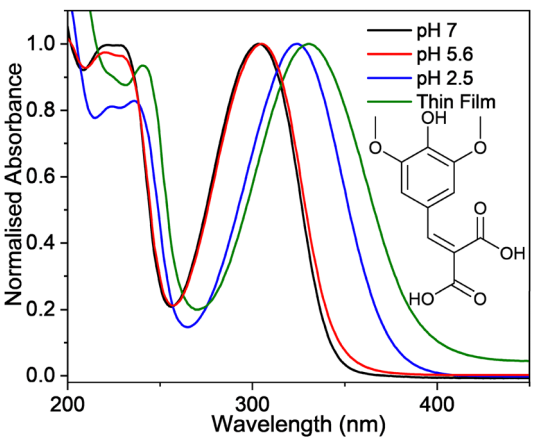

Fig. 1 Steady-state UV/Vis absorption spectrum of SDA in aqueous solution at various pH values and as a thin film sample. The structure of SDA is shown in the inset.

Methods

Experimental methods

Photochemistry: sample preparation. SDA was synthesised through a sustainable green chemistry method previously reported by Rioux *et al.*[15] This method reduces the environmental impact of the synthesis through the use of L-proline as a natural catalyst with moderate heating and reaction time used in its synthesis. Solutions of SDA were prepared in 10 mM concentrations using 0.4 M aqueous sodium phosphate buffer to maintain a physiological pH value of 5.6.[16] Samples of diethyl sinapate, methyl sinapate and sinapoyl malate were made in the previously reported fashion.[17,18]

Wax-coated calcium fluoride (CaF_2) circular windows of 25 mm diameter and 2 mm thickness (UQG optics) were prepared by adapting the protocol previously reported by Pambou *et al.*[19] Specifically, Carnauba wax, no. 1 (CAS: 8015-86-9, Sigma Aldrich) was dissolved in chloroform to a concentration of 0.05% by weight. 1 mL of this solution was then pipetted onto a clean UV grade CaF_2 window and spin-coated using a spin coater (Laurell Technologies, WS-650MZ-23NPP/LITE) programmed to run at 3000 rpm for 20 seconds. These parameters have been shown to give a film thickness between 50 and 100 Å;[19] hence we assume this to be the approximate thickness of the wax coatings on the samples studied in the present work.

Thin films of the chosen sample were then added on top of the wax coatings mentioned above; to achieve this, 1 mL of a 100 mM solution dissolved in ethanol was pipetted on top of a wax-coated CaF_2 window prepared as described above and spun again for 20 seconds at 3000 rpm. The presence of the sample on the surface of the windows was confirmed through UV/Vis absorption spectroscopy, which revealed a peak in the absorption spectrum centred at 330 nm (Fig. 1), approximately 15 nm red-shifted from the absorbance of SDA in aqueous solution at pH 5.6. The thickness of the spin-coated films was calculated through the experimentally determined molar absorption coefficient of SDA, 15 000 ± 2000 M^{-1} cm^{-1}, as shown in the ESI,† Fig. S1. This value of molar absorption coefficient suggests a thickness of approximately 3 μm.

All steady-state UV/Vis absorption spectra were collected on a Cary 60 Spectrometer (Agilent Technologies) using a cuvette of 10 mm path length for solution samples. In addition, the photostability of the samples was assessed by monitoring the absorption spectra of the samples at several time intervals after continuous irradiation with an Oriel instruments, 91 191–1000 solar simulator which was tuned to an irradiation power equivalent to 1 sun (1000 W m^{-2}) using a neutral density filter.

Transient absorption spectroscopy. The TAS set-up used to collect the presented ultrafast spectroscopy data has been described previously;[20,21] hence only specific details about the reported experiments are given here. Photoexcitation (or 'pump') wavelengths were chosen to correspond to the peak absorption wavelength of the samples of interest (305 and 330 nm), with the white light continuum detection (or 'probe') beam (330–740 nm) generated by focussing fundamental (800 nm) laser radiation

into a vertically translated 2 mm CaF_2 window. Liquid samples flowed through the sample interaction region using a diaphragm pump (SIMDOS 02) and a demountable liquid flow cell (Harrick Scientific Products Inc.); PTFE spacers of 100 μm and 6 μm thickness were used to define the thickness of the liquid samples. Thin film samples in liquid form and spin-coated onto the wax surface were translated in the vertical focal plane of the probe beam. Sample degradation in all three environments was monitored by comparing the ΔOD between each scan cycle; if drops in the signal were observed after a scan cycle, the samples were replenished before continuing.

To gain quantitative insight into the ultrafast dynamics of SDA (and SDA^{2-}, *vide infra*), a global sequential fitting method across all probe wavelengths (330–740 nm) was employed using the TIMP package in *R* interfaced through Glotaran.[22,23] Each set of transient absorption spectra collected at a series of pump–probe time-delays (Δt) were sequentially fit with a 3-step kinetic model $\left(i.e.,\ \mathrm{A} \xrightarrow{\tau_1} \mathrm{B} \xrightarrow{\tau_2} \mathrm{C} \xrightarrow{\tau_3} \mathrm{D}\right)$, giving rise to 3 evolutionary associated difference spectra (EADS), each modelling the spectral components associated with a given exponential decay; each EADS exponentially decays with an associated lifetime, τ_n. These exponential decays are convoluted with a Gaussian to model the instrument response function (IRF, ≈ 80 fs full-width half maximum (FWHM)) and a third-order polynomial correction for the chirp of the experimental data.[24] The fit returned lifetimes for each dynamical process, along with associated standard errors reported as twice their value. The fit quality was evaluated through the associated residuals (difference between the fit and the data), displayed in Fig. S2 in Section S2 of the ESI.†

Computational methods. To account for the different environments, DFT and TD-DFT were used to compute sinapic diacid in water (using implicit and explicit solvent models), in the gas phase, and on a mimic of a wax surface (here referred to as model surface). The deprotonated form (SDA^{2-}) was used in aqueous environments, while the neutral (SDA) form was used in the gas phase and model surface calculations, all of which were performed using Gaussian 16 rev a03.[25]

Optimizations and energy calculations of SDA^{2-} and SDA were performed at the ωB97XD/6-31+G(d,p) level (see Fig. S3–S7 and Tables S1 and S2 in Section S3 of the ESI,† for results and further discussion). In the calculations including the model surface, the optimizations were done using ωB97XD/6-31G(d) and subsequent energy calculations using 6-31+G(d,p) basis set. The minimum energy S_1/S_0 state intersections were optimised using the penalty function method proposed by Martínez and co-workers,[26,27] implemented in the CIOpt program with an in-house adaptation to work with Gaussian software. The topographies of the potential energy curves were characterised by linear interpolations in internal coordinates connecting the vertically excited S_1 state (at the ground state equilibrium geometry) to the S_1 minimum and the S_1/S_0 intersection (see Section S3.2 of the ESI†). Charge transfer analysis of the ground and low-lying singlet excited states of neutral and dianionic SDA were computed using the TheoDORE program[28] (see Table S3 in Section S3.3 of the ESI†).

To mimic the water environment, we use SMD (solvation model based on density)[29] as an implicit solvation model (here referred to as $SDA^{2-}\cdot(H_2O)_0$) and systematically added up to 15 water molecules ($SDA^{2-}\cdot(H_2O)_n$, where *n* indicates the number of water molecules). The ground (S_0) and the first three singlet excited electronic states (S_1, S_2, S_3) for SDA^{2-} were optimised with implicit solvation, while the S_0 and S_1 states were optimised with micro-solvation. These SMD/water results can be viewed in Fig. S4 and the reaction coordinates are shown in Fig. S8, in Section S3 of the ESI.†

To simulate SDA in a wax environment, the fully protonated form was considered, since this species is expected to be deposited on the surface. First, optimisations of the S_0 and S_1 states of the isolated neutral SDA molecule in the gas phase were undertaken. Thus, the two most stable conformers of SDA in its ground state (see Fig. S6 and Table S1, ESI†) were selected for the simulations with the wax surface model. The topography of the S_1 state for these isolated conformers is shown in Fig. S10 (ESI†). In the S_0 optimizations of SDA_A and SDA_B in different orientations on the top of the model surface, only the SDA atoms were allowed to move (Fig. S7, ESI†).

Results and discussion

Fig. 1 compares the steady-state UV/Vis absorption spectra of SDA solvated in water at various pH values ranging from pH 2.5, where SDA is fully protonated (pK_a = 2.77), to pH 7, where SDA is dianionic (pK_a = 3.96), demonstrating the sensitivity in absorption maximum (λ_{max}) to pH. Physiological pH of the plant leaf ranges from pH 5–7.[16] Consequently, most of the transient absorption (TA) studies presented below employed SDA solutions buffered to the biologically relevant pH. For completeness, additional TA data were acquired for solutions at pH values outside this range. These data are shown in Section S4 of the ESI.†

TAS studies were performed for SDA in three different environments: (i) SDA dissolved in a solvent, *i.e.* bulk solution; (ii) SDA in bulk solution against a substitute cuticle surface; and (iii) as a thin film, where SDA is deposited on the substitute cuticle. The substitute cuticle surface serves here as a mimic of the real-world application of SDA applied *via* a foliar spray on plant leaves. The TAS data obtained for SDA under environments (i) and (iii) are presented in Fig. 2. The excitation wavelength for each measurement corresponds to the λ_{max} of SDA under the given conditions, as evidenced in Fig. 1.

The TAS measurements for environments (i), shown in Fig. 2a, and (ii), shown in Fig. S12a (ESI†), reveal a similar behaviour following photoexcitation at 305 nm (*i.e.* at λ_{max}), indicating that these photodynamics are driven by bulk effects. Both TAS results, shown in the form of false colour heat maps, display the same features: three excited state absorption (ESA) bands centred at ∼375 nm, ∼425 nm and ∼650 nm, along with a stimulated emission (SE) feature centred at ∼475 nm. All four features decay to reveal a residual ESA centred at ∼390 nm, which is not immediately apparent in the false

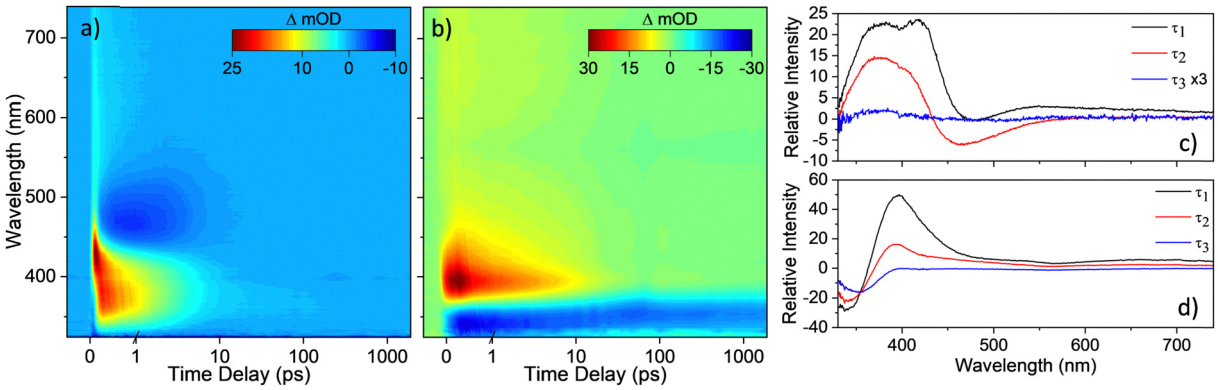

Fig. 2 TAS results displayed as false colour heat maps of (a) bulk aqueous SDA^{2-} solution at pH 5.6 and 10 mM concentration, with a sample path length of 100 μm, photoexcited at 305 nm; (b) a thin film of neutral SDA on top of the substitute wax cuticle surface photoexcited at 330 nm. The time delay is plotted linearly up to 1 ps and then logarithmically to the maximum time delay of 2 ns. Evolutionary associated difference spectra (EADS) extracted from the global sequential fit for: (c) SDA^{2-} at pH 5.6 at 10 mM concentration with a sample path length of 100 μm photoexcited at 305 nm, (d) thin film of SDA on top of the cuticle surface photoexcited at 330 nm.

colour heat maps but is observable in the evolutionary associated difference spectra (EADS) shown in Fig. 2c.

Global sequential fitting of the TAS data also yields similar lifetimes for environments (i) and (ii), presented in Table 1. Interpretation of these data and the associated lifetimes are based on recent studies on sinapoyl malate (SM) and its derivatives, which show efficient relaxation through *trans*/*cis* photo-isomerisation leading to efficient repopulation of the electronic ground state.[30] The symmetric substitution at the terminal carbon in the allylic double bond eliminates the possibility of forming an isomer photoproduct, thereby limiting any possible post-isomerisation reduction in absorption cross-section and any (potential) isomer toxicity.[18,31,32]

Based also on our TD-DFT calculations, these lifetimes are assigned to the following overall mechanism: photoexcitation at 305 nm populates the optically bright $1^1\pi\pi^*$ excited state, from which the molecular geometry relaxes away from the Franck–Condon geometry, within τ_1, reflected by the decay of the ESAs centred at 425 nm and 650 nm. It is likely that τ_1 also includes the time for any solvent reorganisation related to the geometry change as the molecule moves out of the Franck–Condon region.[30,33] The excited (S_1) state population evolves towards the energetically accessible intersection between the S_1 and ground (S_0) states, where it undergoes internal conversion (IC) leading to highly vibrationally excited S_0 state molecules. τ_2 is assumed to encompass the excited state population's evolution along the S_1 state surface, the non-adiabatic coupling to the S_0 state and the subsequent relaxation of the hot S_0 state. Both the ESA (at ~375 nm) and the SE (~475 nm) features decay within τ_2; consistent with the excited-state lifetimes of similar symmetrically substituted systems.[18,31] Despite the present analysis offering no separate lifetime attributable to vibrational cooling in the S_0 state, the TAS data do show some evidence for this process, with a modest blue shifting of the absorption ~375 nm (Fig. 2a, and Fig. S2a in the ESI†).

The third lifetime returned by the fitting, τ_3, persists for the maximum pump–probe time delay in these experiments (Δt = 2 ns) and is assigned to residual population trapped in an excited state. We note here that the long-lived component could alternatively be taken as an indication of photoproduct formation, but we discard this on the grounds that (i) the symmetrical substitution within SDA (and SDA^{2-}) leads to only one ground-state conformer in solution, and (ii) steady-state bulk solution photostability measurements show no visible change in absorbance in this spectral region (≈400 nm) following continuous irradiation with a simulated solar spectrum for 2 h (Fig. 5).

To further explore the excited-state potential energy landscape of SDA (specifically, SDA^{2-} at a pH of 5.6 in aqueous solution), TD-DFT calculations have been undertaken on bare SDA^{2-} and on the SDA^{2-} dianion microsolvated with up to 15 water molecules.[29] These will be identified as SMD/water calculations (where SMD is the acronym for solvation model based on density), (more details of which can be found in Section S3 of the ESI,† particularly in Fig. S3–S5).

The vertical excitation energies were found to vary little as the number of water molecules was augmented (*cf.* the implicit solvation case with no explicit water molecules). Good agreement between the experimental absorption spectrum and the

Table 1 Lifetimes extracted from the global sequential fit of the TAS data along with standard errors. The errors are reported as half of the instrument response when the uncertainty returned by the fitting software is smaller

Environment	τ_1 (fs)	τ_2 (ps)	τ_3 (ns)
(i) Bulk aqueous solution (100 μm) SDA^{2-}	370 ± 40	2.53 ± 0.04	≫ 2
(ii) Bulk solution against cuticle surface (6 μm) SDA^{2-}	360 ± 40	2.44 ± 0.04	≫ 2
(iii) Deposited on Wax SDA	450 ± 40	11.9 ± 0.1	≫ 2

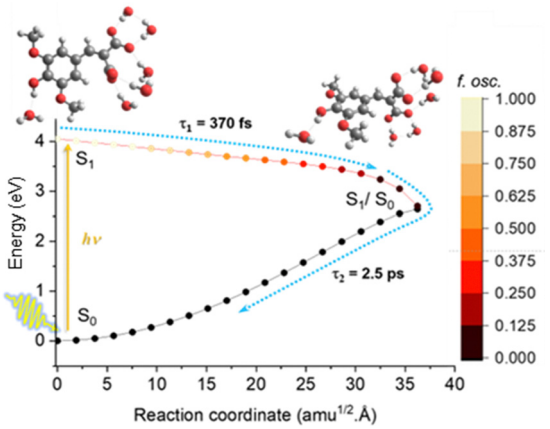

Fig. 3 Reaction coordinate, calculated through linear interpolation of internal coordinates (LIIC) for SDA^{2-} in solution microsolvated with 6 water molecules. The points along the excited-state reaction pathway are colored according to their (relative) oscillator strength for the transition from S_1 to S_0 (denoted *f.osc.*).

computed S_1–S_0 vertical excitation energies was achieved at the ωB97XD/6-31+G(d,p) level of theory. The present calculations show that the phenyl ring and one of the carboxylate groups are coplanar at the minimum energy geometry of the S_0 state parent molecule. The second carboxylate group is near perpendicular to this plane. After excitation to S_1, the allylic bond twists, and the two carboxylate groups are almost perpendicular to the plane of the phenyl ring at the S_1/S_0 intersection geometry. Similar results were reported previously for other symmetrically substituted sinapates.[18,31,34] Fig. 3 (see also Fig. S9 in the ESI†) reveals a barrierless pathway from the Franck–Condon region of the S_1 potential towards the S_1/S_0 intersection. This excited state is initially bright but becomes optically dark, *i.e.* the S_1–S_0 oscillator strength declines to near zero upon approaching the S_1/S_0 crossing geometry. These calculations support the assigned relaxation mechanism of SDA^{2-} *via* a rapid barrierless IC to the S_0 state.

Thin films of SDA were created by applying and spin-drying a solution of SDA dissolved in ethanol onto a wax substrate, which resulted in ∼3 μm thick films (see ESI† for more details). These films on the wax substrate should be better mimics of the environment in which the molecular heater is intended to perform. Following photoexcitation at 330 nm (*i.e.* λ_{max}), the photodynamics of thin films of SDA on wax (Fig. 2b) are revealed by a broad ESA with a prominent maximum centred ∼400 nm, which blue shifts over the first 10 ps as it decays. An apparent red shift in the ground state bleach (GSB) feature after 10 ps is also evident, but this can be rationalised simply by the overlap of the ESA and GSB signals at early time delays. A clear GSB feature is evident at 350 nm, which persists out to Δt = 2 ns. Such long-lived GSB features are often a signature of molecular degradation,[35] but the present thin film samples of SDA are found to retain 70% of their UV/Vis absorbance following 2 h continuous irradiation with a solar simulator, which suggest an explanation other than degradation for the persistence of this GSB feature.

These results are now discussed in the context of the proposed relaxation mechanism for SDA, noting the obvious differences between thin film and solution (see Fig. 2). In the case of the thin film samples of SDA, photoexcitation at 330 nm gives rise to a broad ESA spanning almost the full range of the probe spectrum (350–740 nm) with a maximum at ∼400 nm, along with a GSB centred at 340 nm. These features decay with a lifetime of τ_1, assigned to the S_1 population undergoing geometry relaxation towards the energetically accessible S_1/S_0 intersection, as discussed *supra* for the bulk solution. Here we note the significantly longer τ_2 value (∼12 ps) than found in the bulk solution (∼2.5 ps). This difference could indicate that (i) the S_1 population takes much longer to traverse the S_1/S_0 intersection when on the wax substitute, but the lack of SE signal suggests that IC is rapid, or (ii) the vibrationally hot S_0 molecules cool more slowly in this environment (*i.e.* more frustrated ground state dynamics). Consistent with the latter view, we note that the anionic nature of SDA^{2-} in solution at pH 5.6 may well increase the effectiveness of the energy dissipation (*cf.* the neutral species in a thin film) through the formation of a hydrogen bonding network with water molecules.[36] Finally, τ_3 is assigned from the long-lived GSB centred ∼340 nm, which persists beyond the maximum Δt of 2 ns. While a long-lived GSB feature (usually) is an indication that some excited population has not returned to the initial ground-state minimum energy configuration, there are no additional features to suggest photoproduct formation.

Again, we turn to theory to guide interpretation of the observed TAS data and provide additional insight into the origin of τ_3 in the thin film measurements. Geometry optimisations of neutral SDA were first computed in a vacuum at the ωB97XD/6-31+G(d,p) level of theory. For neutral SDA, the intramolecular hydrogen bond between the two carboxylic groups restricts them to the same plane, but they can assume different orientations, giving rise to different conformers. The most stable two conformers are separated by ∼2 kcal mol^{-1}: SDA_A (the most stable conformer) has the carbonyl group oriented towards the phenyl ring, maintaining overall planarity; whereas SDA_B has the hydroxyl group oriented towards the phenyl ring, losing planarity, which results in a slight shift in the predicted absorption spectrum and slightly different extinction coefficients for the two conformers (Fig. S6 and Table S1 in the ESI†).

Modelling a leaf surface is challenging since it is non-crystalline and varies morphologically and compositionally among plant species.[37] The main components, however, are typically primary and secondary alcohols, ketones, fatty acids and aldehydes with twenty to forty carbon atoms.[38] To simulate the impact of a wax surface on the SDA dynamics, we start with a simple model based on a class of epicuticular wax with platelet morphology, which exhibits single-crystal patterns largely dominated by primary alcohols with carbon chains larger than twenty atoms.[38,39] The chosen model consists of SDA on top of the crystalline structure of 1,21-henicosanediol (extracted from Cambridge Crystallographic Database, deposition number 153917).[40] The SDA_A and SDA_B conformers were optimised in different orientations atop the model surface using TD-DFT, keeping the surface frozen. The two most stable S_0 geometries obtained using this model (SDA_{A1} and SDA_{A2}) are

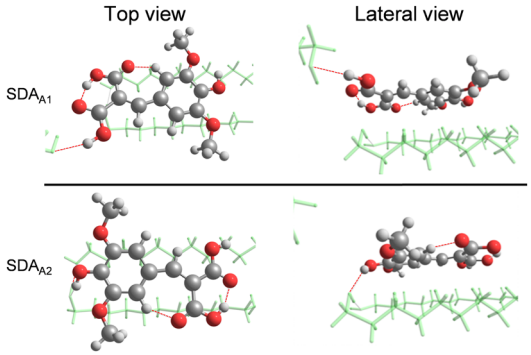

Fig. 4 Optimized ground state geometries of SDA_A deposited on the model surface. Red lines denote the hydrogen bonds. The subscripts A1 and A2 refer to different binding arrangements of SDA on the model surface.

shown in Fig. 4. The most stable, SDA_{A1}, is bonded to the surface dialcohols by a carboxylic acid group of SDA, while SDA_{A2} is bonded to the surface through the phenolic hydrogen (see Fig. S7 and Table S2, ESI†).

Guided by these calculations, we now suggest the origin of τ_3 in the thin film measurements. The most stable conformer, SDA_{A1}, has one of the largest oscillator strengths (Table 2). Following photoexcitation and relaxation to the ground state, some population may relax into other local minima on the S_0 state through a rotation of the allylic group, generating, for example, SDA_{B1}, which has a lower oscillator strength, thus manifesting as a persistent GSB signal in TAS measurements (*viz.* Fig. 2b). No absorption features attributable to such higher energy conformers are identified but this is unsurprising given the similarities in their vertical excitation energies (see Table 2). Finally, we should also consider that the formation of these photoproducts, which could lead to an increased absorption in the >400 nm region, occurs beyond the maximum time window of our experiments (2 ns). As such, we unfortunately

Table 2 Ground state energies (defined relative to the most stable minimum), and S_1–S_0 vertical excitation energies and oscillator strengths for all four conformers of SDA on the model surface

Conformer	S_0 energy, relative to that of SDA_{A1} (kcal mol^{-1})	S_1–S_0 vertical excitation energy (eV nm^{-1})	*f.osc*
SDA_{A1}	0	3.87/320	0.64
SDA_{A2}	5.96	3.63/342	0.68
SDA_{B1}	16.82	3.85/322	0.59
SDA_{B2}	8.22	3.63/342	0.61

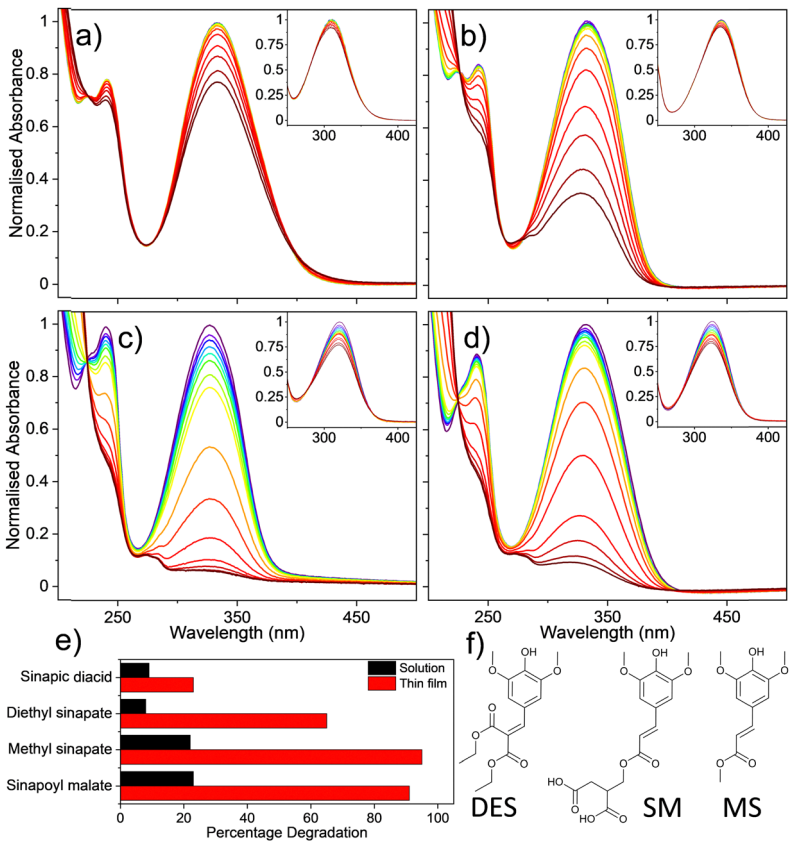

Fig. 5 Normalised UV absorption spectra following continuous solar irradiation (I = 1 sun = 1000 Wm^{-2}) of films deposited from solutions of sinapate based molecules in ethanol on the substitute wax cuticle; inserts show the normalised UV absorption spectra following continuous solar irradiation of bulk solutions of sinapate based molecules in water at pH 5.6 for (a) sinapic diacid, (b) diethyl sinapate, (c) methyl sinapate and (d) sinapoyl malate. The colour bar in panel (a) shows irradiation time in seconds. (e) Bar graph showing the different photodegradations (as a %) at the peak absorption wavelength for different sinapate based molecules. (f) Chemical structures of diethyl sinapate (DES), sinapoyl malate (SM), and methyl sinapate (MS).

do not have the time range to observe any potential transient signals that could be directly attributed to the UV/Vis changes in our steady-state measurements. In summary, the TAS data and TD-DFT calculations reported here show that the absorbed photon energy is rapidly converted to vibrational energy (*i.e.* heat) across all three environments that the SDA molecular heater is likely to encounter on the surface of a leaf.

Another key criterion for commercial use of any molecular heater is its long-term photostability, which is here assessed in solution and on the mimetic cuticle surface. This part of the study was expanded to include several other structurally similar sinapate based molecules to compare the results for SDA against other possible molecular heaters. Comparators discussed here are diethyl sinapate (DES), methyl sinapate (MS) and sinapoyl malate (SM) all of which were dissolved in water as described for SDA. Results for all four samples following 2 h irradiation with a solar simulator (intensity, I = 1 sun = 1000 W m^{-2}) are shown in Fig. 5. Irradiations were only performed for a maximum of 2 h to assess their immediate photostability. While accelerated aging studies would provide a more complete assessment of the samples' photostability over longer periods of time, the heating in such experiments would damage the layer of wax, thus preventing a meaningful study. An alternative approach would be to monitor the degradation of SDA over much longer periods of time at temperatures that replicate real life. Whilst such experiments are time-consuming and beyond the immediate scope of the present work, these could form the focus of a future study. Clearly, SDA presents excellent photostability in solution (Fig. 5a insert), showing only 9% degradation over 2 h irradiation at the absorption maximum. Notably, compared with all other samples, SDA also presents the best photostability (23% degradation under the same irradiation conditions) as a thin film on the wax substitute cuticle. Again, we note that symmetric substitution at the terminal carbon atom in the allylic double bond (in DES and in SDA) results in improved relative photostability on the wax substitute cuticle *cf.* the non-symmetrically substituted molecules MS and SM, Fig. 5c and d. The increased photodegradation (*cf.* SDA) is also obvious from inspecting the respective UV absorption spectra at wavelengths below 250 nm, where DES, MS, and SM each exhibit a much larger increase in UV absorption attributable to photoproduct formation following 2 h irradiation. This provides further evidence of the favourable photostability (resilience to UVR damage) of SDA. We also note that the present predictions of multiple conformers of SDA on the wax surface are consistent with the isosbestic point observed at $\sim$400 nm (see Fig. 5a), where the small increase in absorbance at longer wavelengths is attributed to formation of higher energy conformers, as discussed above. DES, MS and SM do not show this behaviour. While the complete assignment of the degradation products for these molecules is beyond the scope of this work, previous publications have tracked the degradation products for structurally similar molecules,[41] and found multiple degradation products with the main bond cleavage occurring on the ester moiety. The absence of such a group in SDA may explain its increased photostability, compared to the other samples. These studies further demonstrate the critical role of symmetric substitution at the terminal carbon atom in the allylic double bond in boosting photostability of the molecular heater.[18,31,32]

Conclusions

The present study describes a multidisciplinary approach that has led to the shortlisting of SDA as a target molecular heater. SDA has been prepared by a green synthesis route, and its photophysical properties and mechanisms across all environments in which it is intended to work as a molecular heater investigated, with a combination of steady-state and ultrafast laser spectroscopy studies and complementary electronic structure calculations. SDA clearly demonstrates impressive resilience to prolonged irradiation. Foliar sprays containing materials such as SDA could potentially be used to elevate plant temperature, offering a new approach towards boosting crop yields and enabling viable growth over expanded geographic regions, thereby contributing to the Zero Hunger initiative by the United Nations.

Author contributions

J. M. W., N. d. N. R. and V. G. S. acquired and analysed the time resolved spectroscopic data and prepared the first draft of the manuscript. T. T. A. performed and analysed the steady-state spectroscopic data. J. M. T., M. T. do C. and M. B. performed and analysed the (TD)DFT calculations. B. R., M. M. M. and F. A. designed and performed the synthesis and characterisation of the compounds. W. J. B. and M. N. R. A. critically evaluated the entirety of the analysis. C. G., X. S., J. A., M. B., T. M., A. B. and K. F. provided guidance on the broader aspects of the work. All authors contributed to the writing of the manuscript.

Data availability

A data availability statement (DAS) is required to be submitted alongside all articles. Please read our full guidance on data availability statements for more details and examples of suitable statements you can use.

Conflicts of interest

There are no conflicts to declare.

Acknowledgements

The authors acknowledge the FET-Open grant BoostCrop (grant agreement 828753) and the entire BoostCrop (https://boostcrop.eu) team for their interest in the work. The authors also acknowledge the Warwick Centre for Ultrafast Spectroscopy (warwick.ac.uk/research/rtp/wcus/) for the use of the Oriel instruments, 91191-1000 solar simulator and the Cary 60 Spectrometer. N. d. N. R. acknowledges funding from the Fundação para a Ciência e Tecnologia (FCT) under the 5th edition of Stimulus for Individual Scientific Employment Call (Concurso para o Estímulo do Emprego Científico, CEEC).

T. T. A. thanks the University of Warwick for a PhD studentship through the Chancellor Scholarship scheme. M. T. do C., J. M. T. and M. B. thank the Centre de Calcul Intensif d'Aix-Marseille for accessing its high-performance computing resources and the HPC resources from GENCI-TGCC (Grant 2022-A0110813035 and 2023-AD010813035R1). B. R., M. M. and F. A. thank the Agence Nationale de la Recherche (grant number ANR-17-CE07-0046), as well as the Grand Reims, Conseil Départemental de la Marne, and the Grand Est region for financial support. V. G. S. thanks the Royal Society for an Industry Fellowship.

Notes and references

1 R. A. Kerr, *Science*, 2007, **316**, 188–190.
2 G. S. Malhi, M. Kaur and P. Kaushik, *Sustainability*, 2021, **13**, 1–21.
3 E. A. Waraich, R. Ahmad, A. Halim and T. Aziz, *J. Soil Sci. Plant Nutr.*, 2012, **12**, 221–244.
4 R. M. Rivero, R. Mittler, E. Blumwald and S. I. Zandalinas, *Plant J.*, 2022, **109**, 373–389.
5 United Nations, The 17 Goals, **https://sdgs.un.org/goals/goal2**.
6 A. Nesbitt, S. Dorling, R. Jones, D. K. E. Smith, M. Krumins, K. E. Gannon, L. Dorling, Z. Johnson and D. Conway, *Oeno One*, 2022, **56**, 69–87.
7 P. J. Gregory, J. S. I. Ingram and M. Brklacich, *Philos. Trans. R. Soc., B*, 2005, **360**, 2139–2148.
8 L. A. Baker, B. Marchetti, T. N. V. Karsili, V. G. Stavros and M. N. R. Ashfold, *Chem. Soc. Rev.*, 2017, 3770–3791.
9 Y. Wang, L. Zhang and P. Wang, *ACS Sustainable Chem. Eng.*, 2016, **4**, 1223–1230.
10 X. Li, W. Xu, M. Tang, L. Zhou, B. Zhu, S. Zhu and J. Zhu, *Proc. Natl. Acad. Sci. U. S. A.*, 2016, **113**, 13953–13958.
11 R. Li, L. Zhang, L. Shi and P. Wang, *ACS Nano*, 2017, **11**, 3752–3759.
12 M. Gao, L. Zhu, C. K. Peh and G. W. Ho, *Energy Environ. Sci.*, 2019, **12**, 841–864.
13 R. Moore, D. Clark, R. Kingsley and R. Stern, *Botany*, Brown Publishers, 1994.
14 B. Rioux, C. Peyrot, M. M. Mention, F. Brunissen and F. Allais, *Antioxidants*, 2020, **9**, 331.
15 B. Rioux, C. Peyrot, M. M. Mention, F. Brunissen and F. Allais, *Antioxidants*, 2020, **9**, 331.
16 A. R. C. Hass, *Plant Physiol.*, 1941, **16**, 405–409.
17 J. C. Dean, R. Kusaka, P. S. Walsh, F. Allais and T. S. Zwier, *J. Am. Chem. Soc.*, 2014, **136**, 14780–14795.
18 M. D. Horbury, E. L. Holt, L. M. M. Mouterde, P. Balaguer, J. Cebrián, L. Blasco, F. Allais and V. G. Stavros, *Nat. Commun.*, 2019, **10**, 1–8.
19 E. Pambou, Z. Li, M. Campana, A. Hughes, L. Clifton, P. Gutfreund, J. Foundling, G. Bell and J. R. Lu, *J. R. Soc., Interface*, 2016, **13**, 20160396.
20 S. E. Greenough, M. D. Horbury, J. O. F. Thompson, G. M. Roberts, T. N. V. Karsili, B. Marchetti, D. Townsend and V. G. Stavros, *Phys. Chem. Chem. Phys.*, 2014, **16**, 16187–16195.
21 S. E. Greenough, G. M. Roberts, N. A. Smith, M. D. Horbury, R. G. McKinlay, J. M. Żurek, M. J. Paterson, P. J. Sadler and V. G. Stavros, *Phys. Chem. Chem. Phys.*, 2014, **16**, 19141–19155.
22 J. J. Snellenburg, S. P. Laptenok, R. Seger, K. M. Mullen and I. H. M. van Stokkum, *J. Stat. Softw.*, 2012, **49**, 1–22.
23 K. M. Mullen and I. H. M. van Stokkum, *J. Stat. Softw.*, 2007, **18**, 1–46.
24 L. Walmsley, L. Waxer and C. Dorrer, *Rev. Sci. Instrum.*, 2001, **72**, 1–29.
25 M. J. Frisch, G. W. Trucks, H. B. Schlegel, G. E. Scuseria, M. A. Robb, J. R. Cheeseman, G. Scalmani, V. Barone, G. A. Petersson, H. Nakatsuji, X. Li, M. Caricato, A. V. Marenich, J. Bloino, B. G. Janesko, R. Gomperts, B. Mennucci and H. P. Hratchian, *et al.*, *Gaussian 16, Revision A.03*, Gaussian, Inc., Wallingford CT, 2016.
26 B. G. Levine, C. Ko, J. Quenneville and T. J. Martínez, *Mol. Phys.*, 2006, **104**, 1039–1051.
27 B. G. Levine, J. D. Coe and T. J. Martínez, *J. Phys. Chem. B*, 2008, **112**, 405–413.
28 F. Plasser and H. Lischka, *J. Chem. Theory Comput.*, 2012, **8**, 2777–2789.
29 A. V. Marenich, C. J. Cramer and D. G. Truhlar, *J. Phys. Chem. B*, 2009, **113**, 6378–6396.
30 L. A. Baker, M. D. Horbury, S. E. Greenough, F. Allais, P. S. Walsh, S. Habershon and V. G. Stavros, *J. Phys. Chem. Lett.*, 2016, **7**, 56–61.
31 T. T. Abiola, N. d N. Rodrigues, C. Ho, D. J. L. Coxon, M. D. Horbury, J. M. Toldo, M. T. do Casal, B. Rioux, C. Peyrot, M. M. Mention, P. Balaguer, M. Barbatti, F. Allais and V. G. Stavros, *J. Phys. Chem. Lett.*, 2020, **12**, 337–344.
32 T. T. Abiola, B. Rioux, J. M. Toldo, J. Alarcan, J. M. Woolley, M. A. P. Turner, D. J. L. Coxon, M. Telles do Casal, C. Peyrot, M. M. Mention, W. J. Buma, M. N. R. Ashfold, A. Braeuning, M. Barbatti, V. G. Stavros and F. Allais, *Chem. Sci.*, 2021, **12**, 15239–15252.
33 J. M. Woolley, J. S. Peters, M. A. P. Turner, G. J. Clarkson, M. D. Horbury and V. G. Stavros, *Phys. Chem. Chem. Phys.*, 2019, **21**, 14350–14356.
34 J. M. Toldo, M. T. do Casal, M. Barbatti, J. M. Toldo, M. T. do Casal and M. Barbatti, *J. Phys. Chem. A*, 2021, **125**, 5499–5508.
35 J. M. Woolley, R. Losantos, D. Sampedro and V. Stavros, *Phys. Chem. Chem. Phys.*, 2020, **2**, 25390–25395.
36 J. M. Woolley, M. Staniforth, M. D. Horbury, G. W. Richings, M. Wills and V. G. Stavros, *J. Phys. Chem. Lett.*, 2018, **9**, 3043–3048.
37 P. E. Kolattukudy, *Polyesters in higher plants*, Springer, 2001.
38 H. J. Ensikat, M. Boese, W. Mader, W. Barthlott and K. Koch, *Chem. Phys. Lipids*, 2006, **144**, 45–59.
39 K. Koch, B. Bhushan and W. Barthlott, *Prog. Mater. Sci.*, 2009, **54**, 137–178.
40 N. Nakamura, K. Uno and Y. Ogawa, *Acta Crystallogr., Sect. C: Cryst. Struct. Commun.*, 2000, **56**, 1389–1390.
41 B. Rioux, L. M. M. Mouterde, J. Alarcan, T. T. Abiola, M. J. A. Vink, J. M. Woolley, A. A. M. Peru, M. M. Mention, F. Brunissen, G. Berden, J. Oomens, A. Braeuning, V. G. Stavros and F. Allais, *Chem. Sci.*, 2023, **14**, 13962–13978.

